Optical coherence tomography – near infrared spectroscopy system and catheter for intravascular imaging

Ali M. Fard,[1] Paulino Vacas-Jacques,[1] Ehsan Hamidi,[1] Hao Wang,[1,2] Robert W. Carruth,[1] Joseph A. Gardecki,[1] and Guillermo J. Tearney[1,3,4,*]

[1]*Wellman Center for Photomedicine, Harvard Medical School and Massachusetts General Hospital, 55 Fruit Street, Boston, MA 02114, USA*

[2]*Department of Biomedical Engineering, Boston University, Boston, MA 02215, USA*

[3]*Harvard-MIT Division of Health Sciences and Technology, 77 Massachusetts Avenue, Cambridge, MA 02139, USA*

[4]*Department of Pathology, Harvard Medical School and Massachusetts General Hospital, 55 Fruit Street, Boston, MA 02114, USA*

[*]*gtearney@partners.org*

Abstract: Owing to its superior resolution, intravascular optical coherence tomography (IVOCT) is a promising tool for imaging the microstructure of coronary artery walls. However, IVOCT does not identify chemicals and molecules in the tissue, which is required for a more complete understanding and accurate diagnosis of coronary disease. Here we present a dual-modality imaging system and catheter that uniquely combines IVOCT with diffuse near-infrared spectroscopy (NIRS) in a single dual-modality imaging device for simultaneous acquisition of microstructural and compositional information. As a proof-of-concept demonstration, the device has been used to visualize co-incident microstructural and spectroscopic information obtained from a diseased cadaver human coronary artery.

OCIS codes: (110.4500) Optical coherence tomography; (170.6510) Spectroscopy, tissue diagnostics; (110.0113) Imaging through turbid media.

References and links

1. D. Huang, E. A. Swanson, C. P. Lin, J. S. Schuman, W. G. Stinson, W. Chang, M. R. Hee, T. Flotte, K. Gregory, C. A. Puliafito, and J. G. Fujimoto, "Optical coherence tomography," Science **254**(5035), 1178–1181 (1991).
2. J. G. Fujimoto, M. E. Brezinski, G. J. Tearney, S. A. Boppart, B. Bouma, M. R. Hee, J. F. Southern, and E. A. Swanson, "Optical biopsy and imaging using optical coherence tomography," Nat. Med. **1**(9), 970–972 (1995).
3. J. G. Fujimoto, "Optical coherence tomography for ultrahigh resolution in vivo imaging," Nat. Biotechnol. **21**(11), 1361–1367 (2003).
4. R. Leitgeb, C. K. Hitzenberger, and A. F. Fercher, "Performance of Fourier domain vs. time domain optical coherence tomography," Opt. Express **11**(8), 889–894 (2003).
5. K. Goda, A. Fard, O. Malik, G. Fu, A. Quach, and B. Jalali, "High-throughput optical coherence tomography at 800 nm," Opt. Express **20**(18), 19612–19617 (2012).
6. S. H. Yun, G. J. Tearney, J. F. de Boer, N. Iftimia, and B. E. Bouma, "High-speed optical frequency-domain imaging," Opt. Express **11**(22), 2953–2963 (2003).
7. M. Choma, M. Sarunic, C. Yang, and J. Izatt, "Sensitivity advantage of swept source and Fourier domain optical coherence tomography," Opt. Express **11**(18), 2183–2189 (2003).
8. S. H. Yun, G. J. Tearney, B. J. Vakoc, M. Shishkov, W. Y. Oh, A. E. Desjardins, M. J. Suter, R. C. Chan, J. A. Evans, I.-K. Jang, N. S. Nishioka, J. F. de Boer, and B. E. Bouma, "Comprehensive volumetric optical microscopy in vivo," Nat. Med. **12**(12), 1429–1433 (2006).
9. G. J. Tearney, S. Waxman, M. Shishkov, B. J. Vakoc, M. J. Suter, M. I. Freilich, A. E. Desjardins, W.-Y. Oh, L. A. Bartlett, M. Rosenberg, and B. E. Bouma, "Three-dimensional coronary artery microscopy by intracoronary optical frequency domain imaging," JACC Cardiovasc. Imaging **1**(6), 752–761 (2008).
10. S. Waxman, M. I. Freilich, M. J. Suter, M. Shishkov, S. Bilazarian, R. Virmani, B. E. Bouma, and G. J. Tearney, "A case of lipid core plaque progression and rupture at the edge of a coronary stent: elucidating the mechanisms of drug-eluting stent failure," Circ. Cardiovasc. Interv. **3**(2), 193–196 (2010).

#197787 - $15.00 USD Received 17 Sep 2013; revised 27 Oct 2013; accepted 7 Nov 2013; published 6 Dec 2013

11. C. M. Matter, M. Stuber, and M. Nahrendorf, "Imaging of the unstable plaque: how far have we got?" Eur. Heart J. **30**(21), 2566–2574 (2009).
12. G. van Soest, T. Goderie, E. Regar, S. Koljenović, G. L. J. H. van Leenders, N. Gonzalo, S. van Noorden, T. Okamura, B. E. Bouma, G. J. Tearney, J. W. Oosterhuis, P. W. Serruys, and A. F. van der Steen, "Atherosclerotic tissue characterization in vivo by optical coherence tomography attenuation imaging," J. Biomed. Opt. **15**(1), 011105 (2010).
13. T. Kume, T. Akasaka, T. Kawamoto, H. Okura, N. Watanabe, E. Toyota, Y. Neishi, R. Sukmawan, Y. Sadahira, and K. Yoshida, "Measurement of the thickness of the fibrous cap by optical coherence tomography," Am. Heart J. **152**(4), 755e1–755e4 (2006).
14. G. J. Tearney, H. Yabushita, S. L. Houser, H. T. Aretz, I. K. Jang, K. H. Schlendorf, C. R. Kauffman, M. Shishkov, E. F. Halpern, and B. E. Bouma, "Quantification of macrophage content in atherosclerotic plaques by optical coherence tomography," Circulation **107**(1), 113–119 (2003).
15. F. D. Kolodgie, A. P. Burke, A. Farb, H. K. Gold, J. Yuan, J. Narula, A. V. Finn, and R. Virmani, "The thin-cap fibroatheroma: a type of vulnerable plaque: the major precursor lesion to acute coronary syndromes," Curr. Opin. Cardiol. **16**(5), 285–292 (2001).
16. S. Waxman, F. Ishibashi, and J. E. Muller, "Detection and treatment of vulnerable plaques and vulnerable patients: novel approaches to prevention of coronary events," Circulation **114**(22), 2390–2411 (2006).
17. C. V. Felton, D. Crook, M. J. Davies, and M. F. Oliver, "Relation of plaque lipid composition and morphology to the stability of human aortic plaques," Arterioscler. Thromb. Vasc. Biol. **17**(7), 1337–1345 (1997).
18. G. van Soest, E. Regar, T. P. M. Goderie, N. Gonzalo, S. Koljenović, G. J. L. H. van Leenders, P. W. Serruys, and A. F. W. van der Steen, "Pitfalls in plaque characterization by OCT: Image artifacts in native coronary arteries," JACC Cardiovasc. Imaging **4**(7), 810–813 (2011).
19. C. Xu, J. M. Schmitt, S. G. Carlier, and R. Virmani, "Characterization of atherosclerosis plaques by measuring both backscattering and attenuation coefficients in optical coherence tomography," J. Biomed. Opt. **13**(3), 034003 (2008).
20. G. van Soest, T. P. M. Goderie, N. Gonzalo, S. Koljenović, G. L. J. H. van Leenders, E. Regar, P. W. Serruys, and A. F. W. van der Steen, "Imaging atherosclerotic plaque composition with intracoronary optical coherence tomography," Neth. Heart J. **17**(11), 448–450 (2009).
21. C. P. Fleming, J. Eckert, E. F. Halpern, J. A. Gardecki, and G. J. Tearney, "Depth resolved detection of lipid using spectroscopic optical coherence tomography," Biomed. Opt. Express **4**(8), 1269–1284 (2013).
22. G. W. Stone, A. Maehara, A. J. Lansky, B. de Bruyne, E. Cristea, G. S. Mintz, R. Mehran, J. McPherson, N. Farhat, S. P. Marso, H. Parise, B. Templin, R. White, Z. Zhang, and P. W. Serruys; PROSPECT Investigators, "A prospective natural-history study of coronary atherosclerosis," N. Engl. J. Med. **364**(3), 226–235 (2011).
23. C. M. Gardner, H. Tan, E. L. Hull, J. B. Lisauskas, S. T. Sum, T. M. Meese, C. Jiang, S. P. Madden, J. D. Caplan, A. P. Burke, R. Virmani, J. Goldstein, and J. E. Muller, "Detection of lipid core coronary plaques in autopsy specimens with a novel catheter-based near-infrared spectroscopy system," JACC Cardiovasc. Imaging **1**(5), 638–648 (2008).
24. S. Waxman, J. Tang, B. J. Marshik, H. Tan, K. R. Khabbaz, R. J. Connolly, T. A. Dunn, A. F. Zuluaga, S. DeJesus, J. D. Caplan, and E. J. Muller, "In vivo detection of a coronary artificial target with a near infrared spectroscopy catheter," Am. J. Cardiol. **94,** 141E-E (2004).
25. A. F. Zuluaga and S. T. DeJesus, "Miniaturized probes for intracoronary optical spectroscopy through blood," Am. J. Cardiol. **90**, 128H–129H (2002).
26. J. D. Caplan, S. Waxman, R. W. Nesto, and J. E. Muller, "Near-infrared spectroscopy for the detection of vulnerable coronary artery plaques," J. Am. Coll. Cardiol. **47**(8 Suppl), C92–C96 (2006).
27. R. D. Madder, D. H. Steinberg, and R. D. Anderson, "Multimodality direct coronary imaging with combined near-infrared spectroscopy and intravascular ultrasound: Initial US experience," Catheter. Cardiovasc. Interv. **81**(3), 551–557 (2013).
28. A. R. Tumlinson, L. P. Hariri, U. Utzinger, and J. K. Barton, "Miniature endoscope for simultaneous optical coherence tomography and laser-induced fluorescence measurement," Appl. Opt. **43**(1), 113–121 (2004).
29. H. Yoo, J. W. Kim, M. Shishkov, E. Namati, T. Morse, R. Shubochkin, J. R. McCarthy, V. Ntziachristos, B. E. Bouma, F. A. Jaffer, and G. J. Tearney, "Intra-arterial catheter for simultaneous microstructural and molecular imaging in vivo," Nat. Med. **17**(12), 1680–1684 (2011).
30. J. Mavadia, J. Xi, Y. Chen, and X. Li, "An all-fiber-optic endoscopy platform for simultaneous OCT and fluorescence imaging," Biomed. Opt. Express **3**(11), 2851–2859 (2012).
31. S. Liang, A. Saidi, J. Jing, G. Liu, J. Li, J. Zhang, C. Sun, J. Narula, and Z. Chen, "Intravascular atherosclerotic imaging with combined fluorescence and optical coherence tomography probe based on a double-clad fiber combiner," J. Biomed. Opt. **17**(7), 070501 (2012).
32. J. K. Barton, F. Guzman, and A. Tumlinson, "Dual modality instrument for simultaneous optical coherence tomography imaging and fluorescence spectroscopy," J. Biomed. Opt. **9**(3), 618–623 (2004).
33. J. Park, J. A. Jo, S. Shrestha, P. Pande, Q. Wan, and B. E. Applegate, "A dual-modality optical coherence tomography and fluorescence lifetime imaging microscopy system for simultaneous morphological and biochemical tissue characterization," Biomed. Opt. Express **1**(1), 186–200 (2010).
34. R. F. Bonner, R. Nossal, S. Havlin, and G. H. Weiss, "Model for photon migration in turbid biological media," J. Opt. Soc. Am. A **4**(3), 423–432 (1987).

#197787 - $15.00 USD Received 17 Sep 2013; revised 27 Oct 2013; accepted 7 Nov 2013; published 6 Dec 2013

35. W. Cui, C. Kumar, and B. Chance, "Experimental study of migration depth for the photons measured at sample surface," Proc. SPIE **1431**, 180–191 (1991).
36. S. Feng, F.-A. Zeng, and B. Chance, "Photon migration in the presence of a single defect: a perturbation analysis," Appl. Opt. **34**(19), 3826–3837 (1995).
37. S. H. Yun, C. Boudoux, G. J. Tearney, and B. E. Bouma, "High-speed wavelength-swept semiconductor laser with a polygon-scanner-based wavelength filter," Opt. Lett. **28**(20), 1981–1983 (2003).
38. S. M. R. Motaghian Nezam, B. J. Vakoc, A. E. Desjardins, G. J. Tearney, and B. E. Bouma, "Increased ranging depth in optical frequency domain imaging by frequency encoding," Opt. Lett. **32**(19), 2768–2770 (2007).
39. B. D. Goldberg, B. J. Vakoc, W.-Y. Oh, M. J. Suter, S. Waxman, M. I. Freilich, B. E. Bouma, and G. J. Tearney, "Performance of reduced bit-depth acquisition for optical frequency domain imaging," Opt. Express **17**(19), 16957–16968 (2009).
40. S. Lemire-Renaud, M. Rivard, M. Strupler, D. Morneau, F. Verpillat, X. Daxhelet, N. Godbout, and C. Boudoux, "Double-clad fiber coupler for endoscopy," Opt. Express **18**(10), 9755–9764 (2010).
41. S. Y. Ryu, H. Y. Choi, J. Na, E. S. Choi, and B. H. Lee, "Combined system of optical coherence tomography and fluorescence spectroscopy based on double-cladding fiber," Opt. Lett. **33**(20), 2347–2349 (2008).

1. Introduction

Intravascular optical coherence tomography (IVOCT) [1, 2], implemented by frequency-domain OCT (FD-OCT) [2–5] or optical frequency domain imaging (OFDI) [6, 7], provides three-dimensional microscopic images of blood vessels, including coronary arteries, *in vivo* [8, 9]. The ability of IVOCT to capture arterial microstructural detail is potentially very useful in medicine because it enables coronary artery disease (CAD) treatment decisions to be made based on detailed morphologic information, which should result in better interventional outcomes [10–12]. Furthermore, *in vivo* microscopy via IVOCT may provide information, such as presence of macrophage accumulations and thickness of fibrous caps [13, 14], that aids the detection of the so-called "vulnerable plaque" that is a precursor lesion to acute myocardial infarction [15, 16]. Many lives could be saved were these vulnerable plaques to be identified and treated before the onset of a coronary event.

Even though microstructure is an important component of CAD, advancing understanding and improving diagnosis of atherosclerosis requires knowledge of the artery's chemical and molecular composition as well [17]. Compositional information will also resolve ambiguities regarding IVOCT image interpretation [18–20] and could provide improved means for automatic segmentation that can facilitate real-time 3D visualization of OCT data sets. While some chemical data, such as the presence of lipid, may be inferred from interferometric OCT signal [19–21], this information is limited to the penetration depth of IVOCT, which may be superficial, especially in the presence of macrophages and lipid [18]. The limited penetration depth of IVOCT is particularly problematic for vulnerable plaque; natural history studies [22] have shown that information deep within the arterial wall is important for characterization of high-risk coronary lesions. These factors suggest that intravascular imaging is best served by combining IVOCT with an imaging technology that detects chemical/molecular composition deep within the artery wall.

One such imaging technology that could be combined with IVOCT is diffuse near-infrared spectroscopy (NIRS). Intracoronary NIRS has been developed as a standalone imaging modality [23] and is now commercially available and in clinical use [24]. The catheter device is capable of detecting lipid through blood and deep within the artery wall [25, 26]. Recently, NIRS has been combined with intravascular ultrasound (IVUS) to provide co-registered structural and chemical information [27]. However, IVUS does not have the resolution to visualize important microstructures, such as thin fibrous caps and macrophage accumulations that are relevant to vulnerable plaque diagnosis. Furthermore, fluorescence imaging has been demonstrated as a complementary modality for OCT to provide additional information about molecular signatures [28–33]. Endogenous fluorescence imaging based on laser-induced fluorescence spectroscopy can also complement OCT and provide molecular information non-invasively [32, 33]. Nonetheless, exogenous fluorescence imaging requires perturbative chemical labeling of coronary tissue.

#197787 - $15.00 USD Received 17 Sep 2013; revised 27 Oct 2013; accepted 7 Nov 2013; published 6 Dec 2013

In this paper, we describe a dual-modality catheter-based imaging system and catheter for simultaneous microstructural and compositional imaging using co-registered OCT and diffuse near-infrared spectroscopy (NIRS). It integrates IVOCT and NIRS catheters into a single rotationally-scanning imaging device in which illumination and collection apertures are separated. This technology differs significantly from previously reported dual-modality OCT paradigms in which a single fiber and one illumination/collection aperture are used. Our OCT-NIRS system, which employs a single high-speed wavelength-swept light source for both OCT and NIRS modalities, illuminates the tissue through a single-mode fiber and collects the back-scattered OCT light with the same fiber. Another collection fiber within the catheter detects the NIRS light, 1-2 mm from the illumination location. Such a configuration enables NIRS detection in the diffuse regime, allowing tissue spectroscopy to be performed deeper into the tissue [34–36]. As a proof-of-concept demonstration, we present cross-sectional dual-modality images of human coronary arteries *ex vivo*, showcasing the capability of OCT-NIRS to capture spectroscopy information in addition to microstructure.

2. Catheter-based dual-modality OCT and NIRS

2.1. System overview

The optical layout for our dual-modality catheter-based OCT-NIRS is schematically shown in Fig. 1. For OCT, we used optical frequency domain imaging (OFDI) technology, alternatively known as swept-source OCT (SS-OCT) or frequency-domain OCT [4, 6, 7]. The optical source was a wavelength-swept laser that generated broadband sweeps at a repetition rate of 100 kHz with an optical bandwidth of ~106 nm centered at 1282 nm [37], corresponding to an axial resolution of ~10 μm. The source directed light to a fiber-based interferometer, described in detail elsewhere [6, 38]. The interferometer was composed of a 90/10 optical power splitter, two optical circulators, and an acousto-optic frequency shifter in the reference arm, all pigtailed with standard single-mode fibers (SMF-28). The sample arm output of the interferometer was coupled into the core of a double-clad fiber (DCF). In our OCT-NIRS prototype, we used a single-mode fiber with a low-index polymer coating (Nufern, SM-GDF-1550), which also guided the light through its cladding. Essentially, the coating of the DCF acts as the outer-cladding for the waveguide. The DCF was then input into a double-clad fiber coupler built in our lab; it was designed such that the core light experienced a minimal insertion loss (section 2.2). The DCF output of the coupler was directed towards a DCF optical rotary junction (section 2.3) and then the OCT-NIRS catheter (section 2.4).

The OCT-NIRS catheter delivered OCT light to the tissue and collected the back-scattered and diffuse light, from the DCF's core and inner cladding, respectively, as described in section 2.4. Upon return of OCT and NIRS light, the custom-built double-clad fiber coupler extracted the cladding light (NIRS light), while it directed the OCT light back to the interferometer. The NIRS light was then detected using a low-bandwidth InGaAs photo-receiver (NewFocus, 2053-FC). The use of a wavelength-swept laser allowed us to detect the spectrum in the time domain using a single-pixel photo-receiver at high speeds (up to 100,000 spectra per second, equivalent to the source's repetition rate). The OCT interference signal was captured via a polarization-sensitive balanced receiver with a sensitivity of 110 dB [6, 39]. Simultaneous acquisition of OCT and NIRS signals made it possible to obtain one spectrum per each axial scan, facilitating spatial registration of the two data sets.

#197787 - $15.00 USD Received 17 Sep 2013; revised 27 Oct 2013; accepted 7 Nov 2013; published 6 Dec 2013

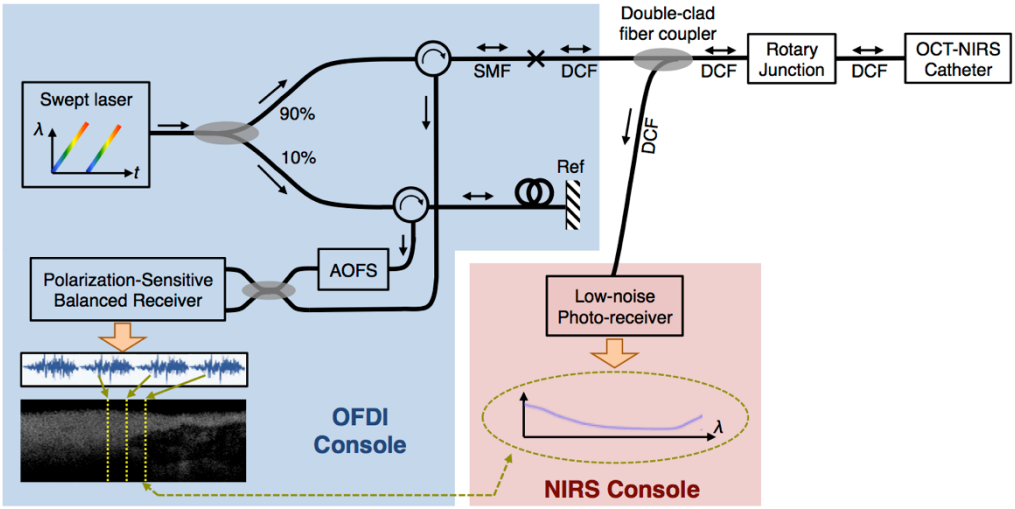

Fig. 1. System diagram for the dual-modality catheter-based optical coherence tomography (OCT) and diffuse near-infrared spectroscopy (NIRS). The OCT-NIRS system consists of OCT/OFDI and NIRS consoles, double-clad fiber coupler, fiber-based rotary junction, and a dual-modal imaging catheter. SMF: Single-mode fiber; DCF: Double-clad fiber; AOFS: Acousto-optic frequency shifter.

2.2. Double-clad fiber coupler

In our OCT-NIRS system, a DCF coupler extracted the NIRS signal that was carried through the inner cladding of DCF. This coupler was designed to allow near-full transmission of the single-mode core light (i.e., OCT signal and NIRS excitation), while it branched off the multi-mode cladding light (i.e., NIRS collection). As discussed earlier, we used a single-mode fiber with a low-index polymer coating (Nufern, SM-GDF-1550) in which the coating acts as the outer-cladding as well. The fabrication process started by stripping fibers' polymer coatings over 15-cm long region. The two fibers were then twisted together (12 turns) and pulled from both ends to ensure their contact. While it was still under tension, the device was inserted and mounted in tubing for protection. Note that the method described here is different from the fabrication method described in [40] by S. Lemire-Renaud et al in which the double-clad fiber had separate outer cladding and coating.

Table 1. Port numbering for the double-clad fiber coupler and their purposes

Port number	*Core / Cladding*	*Purpose*
Port 1	Core	Transceives OCT light to/from catheter
Port 1	Cladding	Receives returned NIRS light from catheter
Port 2	Core	Transceives OCT light to/from OCT console
Port 2	Cladding	Not used
Port 3	Core & Cladding	Transmits NIRS light to NIRS detection console
Port 4	Core & Cladding	Not used

The coupler's performance was measured using a wavelength-swept laser source and a photo-receiver – similar to the scheme used for NIRS signal detection. As illustrated in Fig. 2(a) and summarized in Table 1, when OCT (core) and NIRS (cladding) signals entered through Port 1, NIRS light branched off into Port 3, while the OCT signal was transmitted to Port 2 with minimal insertion loss. Figure 2(b) shows the core's measured signal transmission (red curve) over the operation band (1230 nm – 1330 nm) indicating approximately 0.5 dB insertion loss. It also shows the cladding signal coupling (blue curve), indicating approximately 32% transmission (~4.9 dB) with ~1-dB ripple over the entire band. The coupling ratio is primarily determined by number of turns and length of the coupling region.

#197787 - $15.00 USD Received 17 Sep 2013; revised 27 Oct 2013; accepted 7 Nov 2013; published 6 Dec 2013

It may also be enhanced by slightly fusing the coupling region. Note that our results are in a good agreement with previously published twisting method in [41].

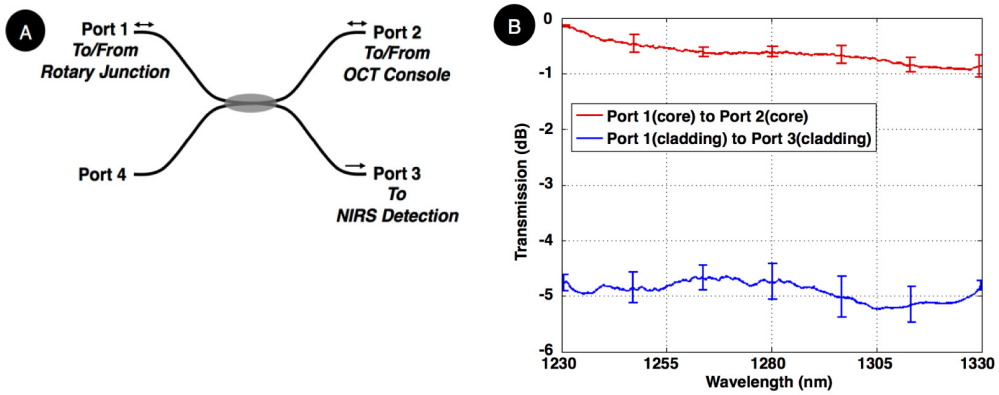

Fig. 2. (A) Double-clad fiber (DCF) coupler schematic, denoting the ports and coupling direction, (B) Transmission spectrum over the operation band. The error bar indicates deviation from the average for four DCF couplers that were fabricated using the described method. The cladding-to-cladding coupling (for NIRS signal) was nearly 4.9 dB, averaged over the entire operation band, while core insertion loss (for OCT signal) was about 0.5 dB.

2.3. DCF optical rotary junction

A DCF optical rotary junction was fabricated to enable circular cross-sectional imaging through a rotationally-scanning catheter. This junction optically coupled light from a static DCF emanating from the DCF coupler to a rotating DCF contained within a driveshaft of the catheter. Inside the rotary junction, the static and rotating DCF were terminated by anti-reflective coated gradient index (GRIN) lenses for free-space beam collimation. The length of the GRIN lenses and their relative positions were optimized to maximize core-to-core coupling of OCT light through DCF for 360-degree full rotation, while they ensure minimal crosstalk between OCT and NIRS light. Note that the rotary junction was terminated by FC/APC connectors to interface with the double-clad coupler and the dual-modality catheter. The fabricated rotary junction had OCT and NIRS insertion loss of 0.6 dB (± 0.3 dB) and 3 dB (± 0.05 dB), respectively. The rotary junction was driven using a motor-drive unit (Micromo, 2232U012SR) with a rotational speed of 1462 RPM, corresponding to 4096 A-lines per cross-section at 100-kHz scan rate.

2.4. Dual-modality catheter

The OCT-NIRS catheter interfaces the DCF rotary junction as schematically shown in Fig. 3. This rotational scanning catheter was composed of a single-mode fiber (OFS, SMM-A1310H) and a multi-mode fiber (Molex, FIP100120140) that were combined into a double-clad fiber (Nufern, SM-GDF-1550) using a commercial optical power combiner (Avensys, MMC02112E). The optical power combiner placed inside the spinning catheter allows light from the multi-mode fiber (MMF) to be coupled to the cladding of the DCF, while it optimally transceived the core light to/from the single-mode fiber (SMF) and the DCF. The DCF was terminated by Diamond E2000 connector to interface with the DCF rotary junction.

At the distal tip, SMF and MMF were terminated by two angle-cleaved ball lenses as shown in Fig. 3 (inset); one that delivered OCT light from the single-mode fiber [numerical aperture (NA) of 0.12] to the tissue and simultaneously collected the back-scattered OCT light from the tissue. The secondary angle-cleaved ball lens was placed at a distant position (~1.5 mm) along the longitudinal direction. This ball lens (with a working distance of 1.5 mm) collected photons that were diffusely transported through the tissue. This configuration can detect tissue contents that are within 500-1500μm depth of the tissue. Note that this

#197787 - $15.00 USD Received 17 Sep 2013; revised 27 Oct 2013; accepted 7 Nov 2013; published 6 Dec 2013

design provides a method to combine the two technologies (OCT and NIRS) into one device. Therefore, one can probe deeper into tissue by increasing the source-detector separation.

The OCT illumination optics at the distal tip of the catheter was designed to provide 30-μm lateral resolution, 10-μm axial resolution, and 1.5-mm working distance. The diffuse light, whose spectrum was modulated by the spectral signature (wavelength-dependent absorption) of the tissue composition, was returned back via the multi-mode fiber with an NA of 0.2. Note that all ball lenses are cleaved at an angle of 38 degrees, resulting in 38 degrees deviation from normal beam incident onto the tissue. This deviation is particularly critical to suppress specular reflection from the tissue surface. On the return path, the commercial optical power combiner coupled the NIRS light into the inner cladding of the double-clad fiber, while the OCT light was transmitted via the core of the same double-clad fiber (single mode propagation).

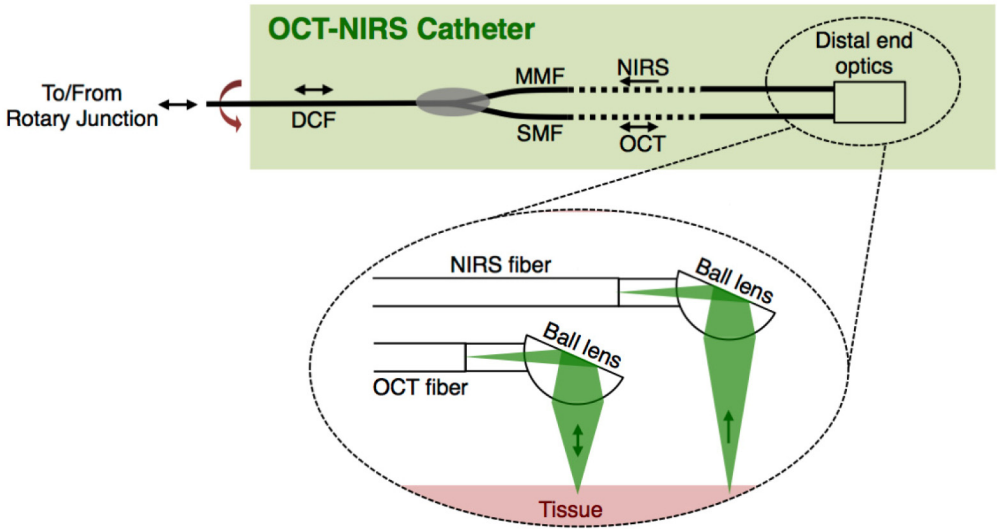

Fig. 3. Schematic for OCT-NIRS catheter. Inside the catheter, a single-mode fiber (SMF) delivered and collected OCT light to/from tissue and a multi-mode fiber (MMF) collected NIRS light. The two fibers were combined into a double-clad fiber (DCF) using a commercial power combiner such that the OCT light transceived through the core of the SMF and DCF, while NIRS light coupled to the cladding of the DCF. At the distal end (insets), the SM and MM fibers were terminated by two angle-cleaved ball lenses for efficient delivery/collection of OCT and NIRS light to/from tissue. In order to spin the catheter for cross-sectional dual-modality imaging, all optical fibers, optical power combiner, and distal optics were housed in a 2.4-Fr driveshaft and stainless steel tubing.

In order to be able to spin the catheter for circumferential cross-sectional dual-modality imaging, the fibers and power combiner were housed in a cardiovascular drive shaft (2.4-Fr diameter) and stainless steel tubing. A transparent plastic sheath (800-μm diameter) was used to enclose the drive shaft and distal optics.

2.5 NIRS data processing

Following photo-detection of the NIRS light, a commercial data acquisition system (NI, USB-6259) operating at a sampling rate of 1.25-MS/s was used to digitize the spectra. The NIRS data processing was performed offline for each imaging session. First, each NIRS reflectance spectrum corresponding to each axial scan was identified based on the OCT A-line number and the number of data points digitized per NIRS spectrum. The first obtained NIRS reflectance spectrum for full data set of the tissue under test was chosen as the reference. By choosing a reference spectrum within the tissue, we can suppress the spectral change resulted

#197787 - $15.00 USD Received 17 Sep 2013; revised 27 Oct 2013; accepted 7 Nov 2013; published 6 Dec 2013

from wavelength-dependent scattering and hence acquire spectral signatures resulted from molecular overtones. All following reflectance spectra in that image were then divided by the reference to remove the spectral background for that frame. The reciprocal of the resultant background-corrected NIRS reflectance spectrum was computed to estimate the NIRS attenuation spectrum. Note that the OCT-NIRS system in fact measures the attenuation of the tissue. Since the scattering is nearly constant over the detection bandwidth and the reference spectrum is chosen within the tissue, we call the resultant NIRS signal "absorption spectra."

3. Results

To demonstrate our catheter-based OCT-NIRS for intravascular imaging, we performed circular cross-sectional scanning of human coronary arteries *ex vivo*. While the OCT sub-system provides axial scanning, full circular cross-sectional information is obtained by spinning the catheter around its rotational axis at a speed of 1462 rpm (corresponding to cross-sectional frame rate of 24 fps). The optical power on the tissue is set to ~16 mW. Both OCT and NIRS data sets were recorded simultaneously such that one NIRS spectra was captured per each OCT A-scan. NIRS data was processed according to the algorithm described in section 2.5.

Fresh human coronary specimens are obtained from National Disease Research Interchange harvested less than 24 hours postmortem. This ex vivo imaging study is approved by the MGH Institutional Review Board (IRB) under the protocol Optical Imaging of Human Vasculature (2004P000578). The sample was prepared by first removing the tissue from a cadaver explant heart. The diseased coronary segment (~3-cm long) was placed on a petri dish during the imaging session. In order to suppress the specular reflection from the tissue, water was injected into the vessel, reducing the refractive index mismatch between the protective plastic sheath and tissue.

Figure 4 shows two cross-sectional OCT-NIRS images of human coronary artery ex vivo, obtained from different longitudinal locations along the artery. The NIRS image (red-hot scale) illustrates the absorption spectra (versus wavelengths) for each A-line. Figure 4(a) shows a lesion at 4 o'clock (denoted by arrow) that has low OCT backscattering. The NIRS image exhibits a flat near-infrared absorption spectra over the lesion. Figure 4(b) shows a cross-section of another lesion (denoted by arrow) that shows low OCT backscattering. Previous studies [21, 26] have shown that the spectra associated with lipid content (e.g. cholesterol) exhibit a negative absorption slope in the near-infrared wavelengths (1200-1400 nm). In the NIRS image [Fig. 4(b)], the area over the lesion appears to have higher absorption (at shorter wavelengths) than elsewhere in the artery. This finding suggests that the plaque in Fig. 4(b) contains abundant lipid. As such, this Fig. 4 demonstrates the capability of NIRS to add complementary information, allowing one to discriminate between two plaques that are similar in appearance by OCT. Note that the distance between the catheter and the tissue surface does not affect the spectral signatures. In future studies, we will derive basis spectra for the chemical constituents in plaques and will conduct Linear Analysis from the measured spectra using these basis functions. This result showcases the ability of our OCT-NIRS catheter and system to acquire microstructural images and associated absorption spectra.

#197787 - $15.00 USD Received 17 Sep 2013; revised 27 Oct 2013; accepted 7 Nov 2013; published 6 Dec 2013

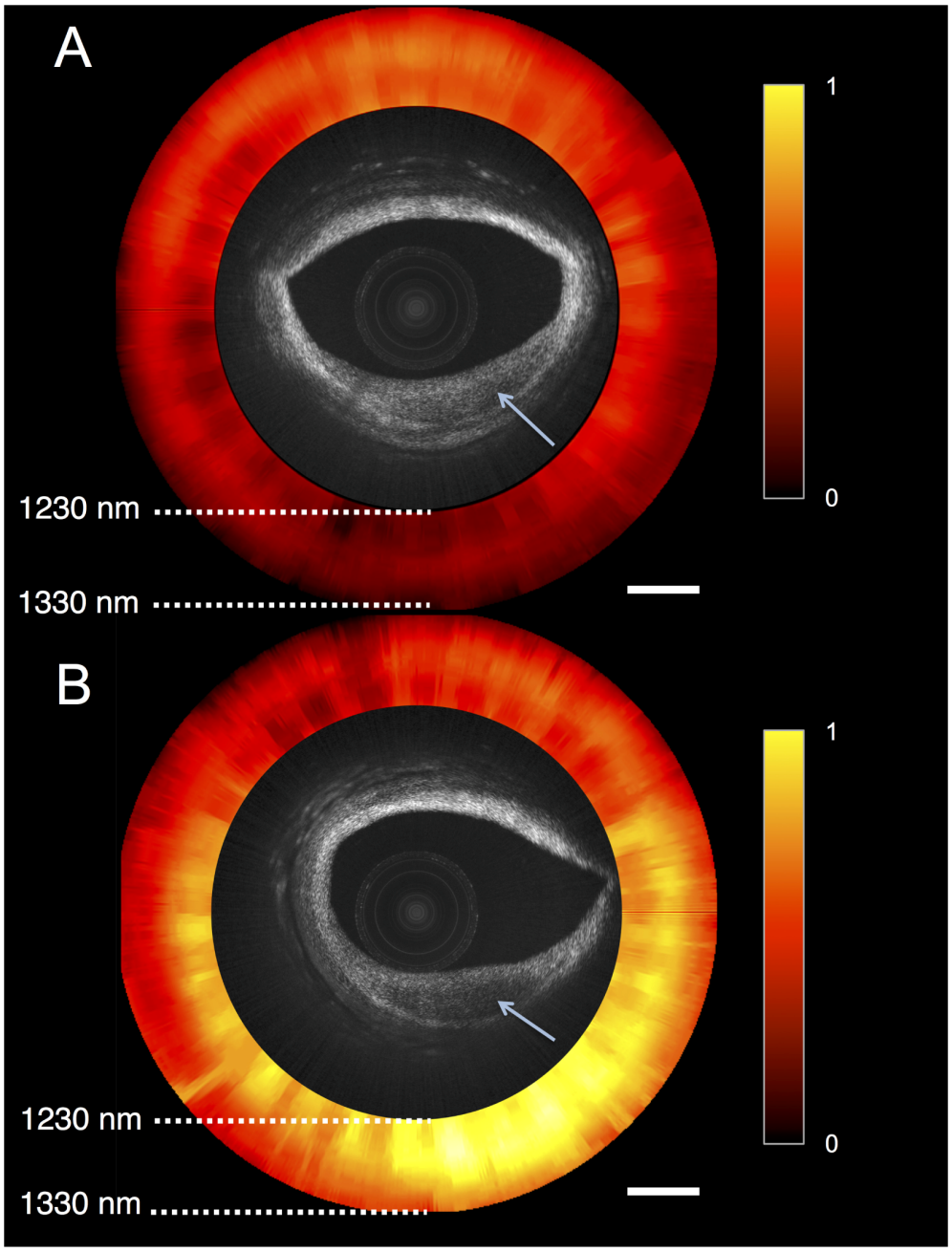

Fig. 4. OCT-NIRS images of cadaver coronary artery ex vivo. Both OCT images show lesions with reduced backscattering. NIRS image shows absorption spectra of tissue versus wavelength, representing the total attenuation normalized for the entire data set; '1' and '0' correspond to the maximum and minimum absorption within the data set, respectively. The NIRS signal in (A) does not demonstrate a high lipid signal, while the NIRS signal in (B) shows the presence of abundant lipid. These findings suggest that the lesion in (A) is does not contain much lipid whereas the lesion in (B) is lipid-rich. Scale bars, 500 µm.

#197787 - $15.00 USD Received 17 Sep 2013; revised 27 Oct 2013; accepted 7 Nov 2013; published 6 Dec 2013

4. Conclusions

We have presented a dual-modality catheter-based optical coherence tomography (OCT) and diffuse near-infrared spectroscopy (NIRS) capable of providing simultaneous microstructural and compositional imaging. This modality combines two complementary imaging and spectroscopy technologies into one device, providing information that will likely enhance visualization, identification, and quantification of tissue contents. As a proof-of-concept demonstration, we showed microstructural images and spectroscopic information obtained from a human coronary artery *ex vivo* at 100-kHz scan rate. In the future, we will modify this technology so that it can be used in human patients and will conduct studies to understand the relationships between OCT and NIRS and the power of combining both in one instrument for coronary artery diagnostics.

Acknowledgments

This work was financially supported by National Institute of Health under grant number R01HL76398 and R01HL093717. Massachusetts General Hospital has a licensing arrangement with Terumo Corporation regarding OFDI technology. Dr. Tearney has the rights to receive royalties as a result of this licensing arrangement.

#197787 - $15.00 USD Received 17 Sep 2013; revised 27 Oct 2013; accepted 7 Nov 2013; published 6 Dec 2013